Flexible optitrode for localized light delivery and electrical recording

S.-T. Lin,[1] J. C. Wolfe,[1] J. A. Dani,[2] and W.-C. Shih[1,*]

[1]*Department of Electrical & Computer Engineering, University of Houston 4800 Calhoun Road, Room N308, Engineering Building 1, Houston, Texas 77204, USA*

[2]*Department of Neuroscience, Baylor College of Medicine, One Baylor Plaza, Houston, Texas 77030, USA*

**Corresponding author: wshih@uh.edu*

Received March 12, 2012; accepted April 1, 2012;
posted April 3, 2012 (Doc. ID 164496); published May 16, 2012

We present optitrode, a miniaturized flexible probe for integrated, localized light delivery and electrical recording. This device features an annular light guide with transparent polymer and fused silica layers surrounding a twisted-wire tetrode. We have developed a novel fabrication process, V-groove guided capillary assembly, to achieve high-precision, coaxial alignment of the various layers of the device. Optitrode with a length-to-diameter ratio ~500 (5 cm long, 100 μm diameter) has been fabricated, and both the electrical and optical functions have been characterized. The prototype can deliver 11% (110 mW) of the total laser power under abrupt bending angle ~25°.

OCIS codes: 220.4000, 230.4685, 230.3990.

The twisted-wire tetrode (TWT) for neuronal unit recording in the deeper regions of the brain, such as the hippocampus, has been indispensible to our understanding of how the neural mechanisms underlying normal learning and memory are usurped by drug addiction or disrupted by neuronal diseases [1,2]. This simple device is fabricated by twisting four ~13 μm insulated nickel-chrome wires together, thermally fusing the insulation, and clipping the end to create a probe with four closely spaced electrodes in a plane perpendicular to the cut wires. This letter describes the integration of a high-efficiency optical channel to deliver light to the sensing electrodes of a TWT while maintaining the fundamental flexibility of the TWT. Such a device could be used for molecularly specific control of *in vivo* neural activities by optogenetic stimulation and silencing [3] with simultaneous electrical recording, which are essential for potential closed-loop feedback control [4].

Since the brain is such a delicate organ, there are several key design goals for a deep-brain probe, including, functionality, miniaturization, biocompatibility, and long-term reliability. Existing approaches of integrated optoelectronic probes are briefly reviewed here: one is to glue a thinned optical fiber to the shank of a silicon probe [5]. Another employs a pulled, dual-core optical fiber combining a graded index optical fiber and a hollow core filled with electrolytes [6]. Another approach builds an integrated waveguide on a silicon probe [7]. There are several limitations with the existing approaches: light propagation loss is very high (>2.2 dB/cm), the structures are rigid compared to the flexible TWT, and the maximum penetration depth is typically much less than 1 cm, as compared to a few inches for the TWT. In this letter, we present a novel device, called an optitrode, to address all these limitations [8].

To take advantage of the existing TWT recording technology, we have developed a precision micro-assembly fabrication process to integrate a TWT into a flexible light guide that features annular cladding/core/cladding structures, as shown in the inset of Fig. 1(a). Our first-generation probe is cylindrical and has an outer diameter (OD) of 100 μm throughout its ~5 cm length. The optitrode is nearly free-standing when one end is held, and its flexibility is shown in Fig. 1(a). The optitrode can be snaked through a head-mounted micro-drive for studying freely moving rats (Fig. 1(b)).

To fabricate the optitrode, we first assemble a home-made TWT into a commercial fused silica microcapillary (Polymicro) using "glue" (Fig. 2a–b). Once the glue is cured (Fig. 2c–d), the protective polyimide jacket is removed by 100 °C sulfuric acid (H_2SO_4), followed by a timed hydrofluoric (HF) acid etching (~1.2 μm/min, 49%) of the microcapillary down to a desired diameter within ±1 μm (Fig. 2e–f). The as-fabricated structure is then assembled into a second glue-filled microcapillary, cured, and polyimide removed. A second HF etching is then applied to remove the second microcapillary completely, resulting in the final device. By appropriate selection of the microcapillary inner and outer diameters, this process can in principle be repeated many times. All assembly has been performed on a 4-inch silicon wafer with aligned two-level V-grooves by which the inner and the outer microcapillaries are centered coaxially, an essential requirement for a uniform outer cladding layer. These potassium hydroxide (KOH)-etched V-grooves are custom made by Nanostructures, Inc.

Polydimethylsiloxane (PDMS) has been employed as a multipurpose material: (1) as the glue during the assembly process for its excellent gap-filling capability; (2) as the cladding material for its excellent optical clarity and

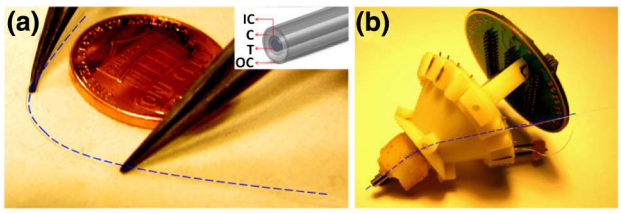

Fig. 1. (Color online) (a) Flexible optitrode; inset shows the cross-sectional view: tetrode (T), inner cladding (IC), core (C), and outer cladding (OC); (b) optitrode snaked through a tetrode micro-drive for studying free-moving rats.

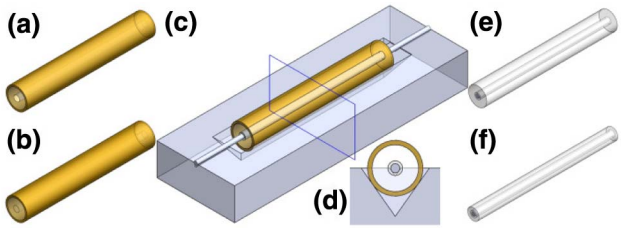

Fig. 2. (Color online) VGCA: (a) capillary; (b) fill capillary with PDMS; (c) curing on two-level V-groove; (d) cross-sectional view of VGCA; (e) remove polyimide by hot H_2SO_4; (f) etch silica by HF.

lower index than fused silica; and (3) as a flexible, protective coating due to its mechanical properties and low toxicity. PDMS is widely used as structural material in microfluidics [9], integrated optical waveguides, and biomedical applications. Since the capillary filling rate decreases significantly with smaller microcapillaries, we have employed a syringe pump to perform pressure-driven ($\mathbf{\Delta p} \sim 1$ atm) filling and it has successfully filled the gap between TWT and microcapillary. The PDMS can be cured in 48 hours under room temperature.

PDMS has a refractive index about 1.4 for ~633 nm light, smaller than that of fused silica ($n = 1.46$), giving rise to total internal reflection (TIR) at both the inner and outer core/cladding boundaries. Since such an annular TIR structure is not well studied, we have performed numerical simulations to investigate the light-guiding performance at 633 nm using the beam propagation method. The first design has a single PDMS layer coated over a 50 μm microwire to a total diameter of 100 μm. This is the simplest form of optitrode without TIR and can be fabricated by one VGCA step. The second design has complete TIR index guiding via the PDMS-silica-PDMS composite layer on the same microwire. Referring to Fig. 1, the outer diameters of the PDMS-silica-PDMS layers are 67, 80, and 100 μm (± 1 μm), respectively. In other words, the effective thickness of the inner cladding, core, and outer cladding layers are 8.5, 6.5, and 10 μm, respectively. These values are selected to match those of the fabricated optitrode discussed later. It is interesting to note that the single PDMS layer design could be an effective device; however, its performance is sensitive to the angle of incidence, the quality of the PDMS layer, and the attenuation and scattering at the metal microwire (Fig. 3(a)). In contrast, we observe robust TIR guiding in the fused silica layer at various angles of incidence, as shown in Fig. 3(b) for the PDMS-silica-PDMS design. The propagation loss is ~0.5 dB/cm in the entire composite layer at ~10° incidence. Figure 3(c) shows that the light in the core propagates steadily but fluctuates and decreases significantly in the cladding layers. As shown in Fig. 3c–d, ~30% of the total coupled light can be guided in the silica core for 5 cm with little dependence on the angle of incidence. In all simulations, the intensity values have been normalized to the total light intensity coupled into the structure. We use a simple Gaussian beam with 100 μm beam waist at the optitrode entrance. Thus, 23% of the input is coupled into the composite layer.

Fig. 4(a) shows a TWT (~50 μm OD) assembled inside a microcapillary with 67 μm ID and 150 μm OD

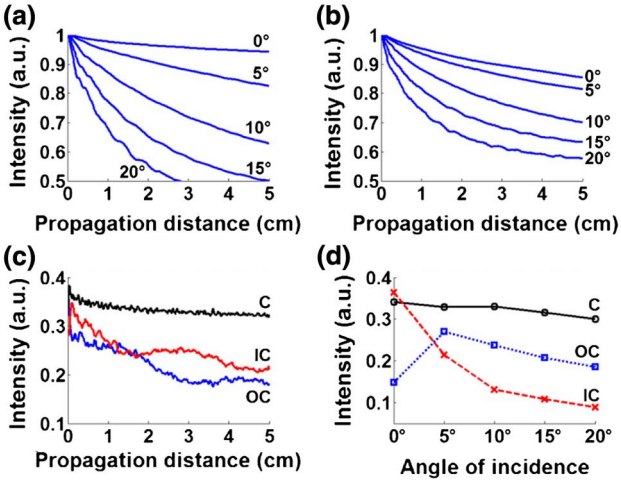

Fig. 3. (Color online) Total intensity vs. propagation distance for various incidence angles for a single-PDMS layer on microwire (a) and for a PDMS-silica-PDMS composite layer on microwire (b); (c) intensity distribution averaged over the five incidence angles in (b); (d) intensity distribution after 5 cm propagation vs. incidence angle for the design in (b).

(polyimide coating included), sitting on the two-level V-groove jig. The OD 80 μm intermediate structure after HF etching is then inserted into the second microcapillary (ID 100 μm, OD 360 μm, polyimide included) and filled. Since this PDMS layer will become the protective layer and the outer cladding, its thickness uniformity is critical and requires VGCA. After curing, the second microcapillary is completely removed, resulting in the final device of OD 100 μm with internal structures shown in Fig. 4(b) throughout its ~5 cm length. Since both PDMS and TWT can be damaged by HF and H_2SO_4, both ends of the optitrode are kept outside the etching solutions during all steps. Although the resulting fused silica thickness (6.5 μm) is thinner than that of outer PDMS layer (10 μm), fused silica core appears to be much thicker under the

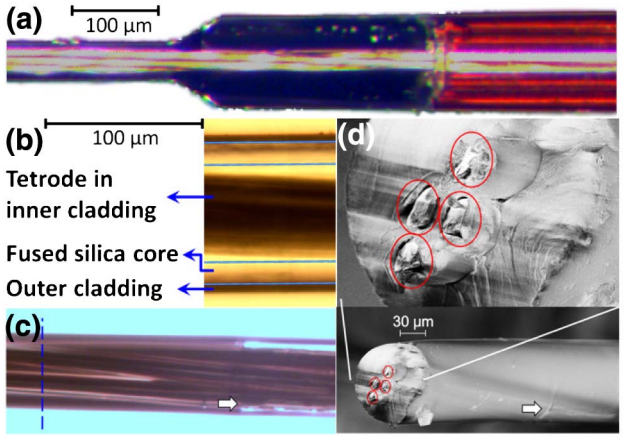

Fig. 4. (Color online) (a) Right end of a 50 μm TWT is inside a PDMS-filled OD 150 μm capillary set in a deeper V-groove, and the left end of the TWT sits in a shallower V-groove; (b) completed optitrode with PDMS-Silica-PDMS layer surrounding a TWT; (c) probe tip image: dashed line shows the final cut position, ~300 μm to the left of the edge of the silica core marked by a white arrow; (d) TWT electrodes are circled in the cross-sectional view after cutting. Tip is facing left, and the arrows indicate the silica core edge.

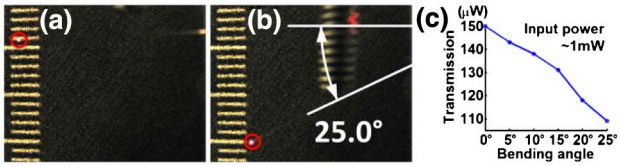

Fig. 5. (Color online) (a–b) Transmission at 0° and 25° bends; (c) transmission measurement 0° to 25°.

microscope due to the projected view of the cylindrical structures. We designed a biocompatibility tip, as shown in Fig. 4c–d, where only the TWT tip is exposed and is ~300 μm in front of the silica core edge in this particular design.

We have tested the optitrode by coupling the output of a 633 nm He-Ne laser (1 mW) into one end using a 40× objective lens and measured from the other end using a calibrated power meter (Ophir, PD300-1W ROHS). We note that the optitrode can be directly coupled to an optical fiber via a connector for experiments with living animals. The exiting light has a numerical aperture ~0.12, with minor isotropic scattering due to the tip roughness. The tip quality can be improved by using a better capillary cleaver and precision grinding or etching. Fig. 5(a) shows 150 μW transmitted light, ~15% of the laser total power exiting a straight 5 cm device. We note that the major loss appears to occur at the coupling stage due to the tetrode blocking a significant portion of the Gaussian beam, not due to the light guide loss. This agrees with our simulation results discussed earlier. The tip power density is ~25 mW/mm^2, which is sufficient for optical stimulation of neurons [10]. Next, we tested the light-guiding performance of optitrode under various abrupt bending angles up to 25°. The results shown in Fig. 5(c) suggest that ~11% of the total laser power can be transmitted, even at an abrupt bending angle as large as 25°. We note that an optical fiber would likely break at this angle if its protective coating is removed. In addition, a bare optical fiber is extremely fragile and difficult to work with. The structural integrity of optitrode is mainly provided by TWT. Both the inner and outer PDMS layers improve the structural flexibility and provide protection against pinching damage by tweezers.

We have measured the impedance of each individual microelectrode of the tetrode at 1 kHz using an impedance meter (A-M Systems, Model 2900). The contact impedance at the microelectrode and electrolyte (0.9% w/v of NaCl solution) interface is ~1.35 ± 0.15 MΩ, agreeing with the theoretical value. An additional electroplating step is typically involved to decorate the tetrode surface with rough gold nanostructures for impedance reduction, a key step for improving the recording signal-to-noise ratio for single unit recording.

In conclusion, we have described the design and fabrication of the flexible optitrode for localized light delivery and electrical recording. The optitrode features a TWT integrated inside a flexible light guide with annular cladding/core/cladding structures. The optical simulations demonstrate robust TIR performance of the light guide with respect to various incidence angles, and the light distribution in different layers at the exit. To fabricate the optitrode, we have developed the VGCA process and demonstrated its efficacy in nearly alignment-free co-centering of multiple cylindrical structures over a length of 5 cm. PDMS has been selected for multiple innovative functions, including the glue during assembly, the inner and outer cladding for the annular TIR light guide, a mechanically flexible structural material, and a biocompatible protective layer. Although the prototype is 100 μm, we have already fabricated a 75 μm optitrode, and are progressing toward one of 50 μm. Ultimately, the size would be limited by the increased resistance in capillary suction of PDMS for smaller diameters, as well as the TWT size. The optitrode may be applied to deep-brain stimulation and recording in living animals.

Wei-Chuan Shih acknowledges funding support from the National Science Foundation (NSF) CAREER Award (CBET-1151154) and Cullen College of Engineering at the University of Houston. John C. Wolfe and John A. Dani acknowledge a seed grant from the Alliance of Nanohealth (ANH).

REFERENCES

1. C. M. Gray, P. E. Maldonado, M. Wilson, and B. McNaughton, J. Neurosci. Methods **63**, 43 (1995).
2. T. Zhang, L. Zhang, Y. Liang, A.G. Siapas, F.-M. Zhou, and J.A. Dani, J. Neurosci. **29**, 4035 (2009).
3. F. Zhang, L.-P. Wang, M. Brauner, J. F. Liewald, K. Kay, N. Watzke, P. G. Wood, E. Bamberg, G. Nagel, A. Gottschalk, and K. Deisseroth, Nature **446**, 633 (2007).
4. K. Deisseroth, Nat. Methods **8**, 26 (2011).
5. S. Royer, B. V. Zemelman, M. Barbic, A. Losonczy, G. Buzsaki, and J. C. Magee, Eur. J. Neurosci. **31**, 2279 (2010).
6. Y. LeChasseur, S. Dufour, G. Lavertu, C. Bories, M. Deschenes, R. Vallee, and Y. De Koninck, Nat. Methods **8**, 319 (2011).
7. I.-J. Cho, H. W. Baac, and E. Yoon, in *IEEE 23rd International Conference on Micro Electro Mechanical Systems (MEMS)*, pp. 995–998 (2010).
8. S.-T. Lin, M. Gheewala, J. C. Wolfe, J. A. Dani, and W.-C. Shih, in *5th International IEEE/EMBS Conference on Neural Engineering (NER)*, pp. 700–703 (2011).
9. J. C. McDonald and G. M. Whitesides, Acc. Chem. Res. **35**, 491 (2002).
10. F. Zhang, L.-P. Wang, E. S. Boyden, and K. Deisseroth, Nat. Methods **3**, 785 (2006).